Spectral Symmetry Analysis

Michael Chertok and Yosi Keller

Abstract—We present a spectral approach for detecting and analyzing rotational and reflectional symmetries in *n*-dimensions. Our main contribution is the derivation of a symmetry detection and analysis scheme for sets of points in $\mathbb{R}^n$ and its extension to image analysis by way of local features. Each object is represented by a set of points $S \in \mathbb{R}^n$, where the symmetry is manifested by the multiple self-alignments of S. The alignment problem is formulated as a quadratic binary optimization problem, with an efficient solution via spectral relaxation. For symmetric objects, this results in a multiplicity of eigenvalues whose corresponding eigenvectors allow the detection and analysis of both types of symmetry. We improve the scheme's robustness by incorporating geometrical constraints into the spectral analysis. Our approach is experimentally verified by applying it to 2D and 3D synthetic objects as well as real images.

Index Terms—Computer vision, symmetry detection, optimization, spectral relaxation.

1 Introduction

Symmetry detection and analysis is a fundamental task in computer vision. Most man-made and biological objects exhibit symmetry to some extent. For instance, consider artificial objects such as airplanes and houses or natural ones such as fish and insects. Thus, symmetry is a ubiquitous phenomenon and a useful cue for visual recognition. This is supported by experimental analysis of perceptual grouping and attention of the human visual system [1].

The two most common types of symmetries are rotational and reflectional symmetries. An object is said to have rotational symmetry of order K if it is invariant under rotations of $\frac{2\pi}{K}k$, $k = 0 \dots K-1$, about a point denoted the *symmetry center*, whereas an object has reflectional symmetry if it is invariant under a reflection transformation about a line, denoted the *reflection axis*. Fig. 1 presents both types of symmetry.

Over the years, a myriad of approaches were suggested for symmetry analysis [2], [3], [4], [5], [6], [7], [8], [9], [10]. Most of them deal with 2D symmetries, while a few analyze 3D data [4]. A recent survey [11] by Chen et al. found that despite the significant research effort made, there is still a need for a robust, widely applicable "symmetry detector."

In this work, we propose a computational approach to the detection and analysis of symmetries in an n-dimensional sets of points. Our approach is based on the self-alignment of points using the spectral relaxation scheme proposed by Leordeanu in [12].

Our core contribution is to show that the symmetry of a sets of points $S \in \mathbb{R}^n$ is manifested by a multiplicity of the leading eigenvalues and corresponding eigenvectors. This leads to a purely geometric symmetry detection approach that only utilizes the *coordinates* of the set S, and can thus be applied to abstract sets of points in $\mathbb{R}^n$. Given the eigendecomposition, we show how to recover the intrinsic properties of reflectional and rotational symmetries (center of rotation, point correspondences, and symmetry axes).

As our second contribution, we derive a geometrical pruning measure by representing the alignments as geometrical transforms in $\mathbb{R}^n$ and enforcing a determinant value constraint on their representation as matrices. This allows us to reject erroneous matchings and analyze real data, where symmetries are often embedded in clutter.

As our third contribution, we analyze the case of perfect symmetry and show that it results in a degenerate eigendecomposition. We then resolve this issue and explain why perfect symmetry rarely appears in real data such as images.

The proposed scheme requires no a priori knowledge of the type of symmetry (reflection/rotation) and holds for both. Our scheme, denoted as Spectral Symmetry Analysis (SSA), can detect partial symmetry and is robust to outliers.

As our last contribution, we apply the SSA to the analysis of symmetry in images, for which we utilize local image features [13], [14] to represent images as sets of points. We also utilize image descriptors to reduce the computational complexity. The research in this field is significant and is of particular interest to us.

The paper is organized as follows: We start by presenting the geometrical properties of symmetries in Section 2 and then survey previous results on symmetry detection, local features, and spectral alignment in Section 3. Our approach to symmetry analysis is presented in Section 4 and experimentally verified in Section 5. Concluding remarks are given in Section 6.

2 Symmetries and their Properties

In this work, we study the symmetry properties of sets of points $S = \{x_i\}$ such that $x_i \in \mathbb{R}^n$. The common types of symmetries are the rotational and reflectional symmetries. Sets having only the first type are described by the cyclic group C_K, while others have both rotational and reflectional symmetry and are described by the dihedral group D_K, where K is an order of the respective symmetry.

In this section, we define the rotational (cyclic) and reflectional (dihedral) symmetries, denoted C_K and D_K,

• *The authors are with the School of Engineering, Bar Ilan University, Ramat Gan, Israel. E-mail: {michael.chertok, yosi.keller}@gmail.com.*

Manuscript received 3 July 2008; revised 5 Jan. 2009; accepted 6 May 2009; published online 18 May 2009.
Recommended for acceptance by M. Lindenbaum.
For information on obtaining reprints of this article, please send e-mail to: tpami@computer.org, and reference IEEECS Log Number TPAMI-2008-07-0396.
Digital Object Identifier no. 10.1109/TPAMI.2009.121.

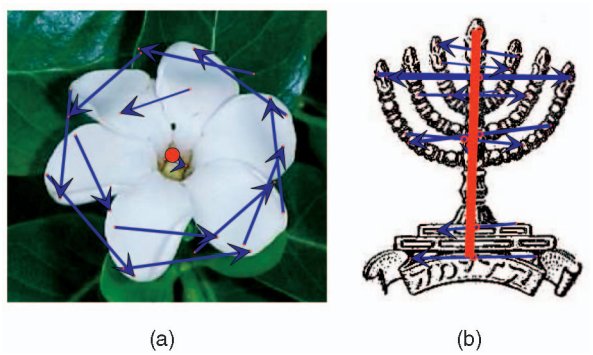

Fig. 1. Rotational and reflectional symmetries. (a) Rotational symmetry of order six without reflectional symmetry. (b) Reflectional symmetry of order one.

respectively. By considering the subsets of points $\{S_I^C, S_I^D\} \subset S$ that are invariant under the corresponding symmetry transforms T_{C_K} and T_{D_K}, we are able to recover the rotation centers and reflection axes. These invariant sets are shown to be related to the spectral properties of T_{C_K} and T_{D_K}. Finally, we derive an analytical relationship between T_{C_K} and T_{D_K} in a 2D case, which allows us to infer the rotational symmetry transform T_{C_K}, given two reflectional transforms T_{D_K}.

2.1 Rotational Symmetry

Definition 1 (Rotational symmetry). *A set $S \in \mathbb{R}^n$ is rotationally symmetric with a rotational symmetry transform T_{C_K}, of order K if $\forall x_i \in S, \exists x_j \in S$, s.t.*

$$x_j = T_{C_K} x_i. \tag{1}$$

For $S \in \mathbb{R}^2$, T_{C_K} is given by

$$T_{C_K}(x, y) = \begin{pmatrix} \cos\beta_k & -\sin\beta_k & 0 \\ \sin\beta_k & \cos\beta_k & 0 \\ 0 & 0 & 1 \end{pmatrix} \begin{pmatrix} x \\ y \\ 1 \end{pmatrix}, \tag{2}$$

where $\beta_k = \frac{2\pi}{K} k$, $k = 0, \ldots, K-1$. Thus, for a symmetry of order K, there exists a set of K transformations $\{R_{\beta_k}\}_1^K$ for which (1) holds. The use of homogeneous coordinates in (2) allows us to handle noncentered symmetries.

An example of rotational symmetry is given in Fig. 1a. Equation (2) implies that

$$\det(T_{C_K}) = 1, \tag{3}$$

where the invariant set S_I^C is the center of rotational symmetry.

Given a rotation operator T_{C_K}, the center of rotation (that is also the center of rotational symmetry) X_c is invariant under T_{C_K} and can be computed as the eigenvector of T_{C_K} corresponding to the eigenvalue $\lambda = 1$:

$$T_{C_K} X_c = X_c. \tag{4}$$

2.2 Reflectional Symmetry

Definition 2 (Reflectional symmetry). *A set $S \in \mathbb{R}^n$ is reflectionally symmetric with respect to the vector (reflection axis) $\langle \cos\alpha_0, \sin\alpha_0 \rangle$ with a reflectional transform T_{D_K}, if $\forall x_i \in S, \exists\, x_j \in S$, s.t.*

$$x_j = T_{D_K} x_i, \tag{5}$$

where, for $x_i \in \mathbb{R}^2$, T_{D_K} is given by

$$T_{D_K}(x, y) = \begin{pmatrix} \cos 2\alpha_0 & \sin 2\alpha_0 & 0 \\ \sin 2\alpha_0 & -\cos 2\alpha_0 & 0 \\ 0 & 0 & 1 \end{pmatrix} \begin{pmatrix} x \\ y \\ 1 \end{pmatrix}. \tag{6}$$

A set S has reflectional symmetry of order K if there are K angles α_k that satisfy (5).

An example of reflectional symmetry is given in Fig. 1b, where α_0 is the angle of the reflection axis, and (6) implies that

$$\det(T_{D_K}) = -1. \tag{7}$$

Similarly to the rotational symmetry case, the points on the symmetry axis form an invariant set X_R that corresponds to the eigenspace of

$$T_{D_K} X_R = X_R. \tag{8}$$

Conversely to (4), the eigenspace corresponding to $\lambda = 1$ is of rank 2, in accordance with S_I^D being a line.

2.3 Interrelations between Rotational and Reflectional Symmetries

Theorem 1. *If a set S has rotational symmetry of order K, then it either has reflectional symmetry of order K or has no reflectional symmetry at all [15], [16]. If S has both rotational and reflectional symmetry, then the axes of reflectional symmetry are given by*

$$\alpha_n = \alpha_0 + \frac{1}{2}\beta_k, \qquad k = 0, \ldots, K-1, \tag{9}$$

where α_0 is the angle of one of the reflection axes and β_k are the angles of rotational symmetry.

Theorem 2. *Given two distinct reflectional transforms T_{D_1} and T_{D_2}, one can recover the corresponding symmetrical rotational transforms T_{C_K}:*

$$T_{C_K} = T_{D_1} \cdot T_{D_2}. \tag{10}$$

The proof is given in the Appendix.

2.4 Discussion

The geometrical properties presented above pave the way for a computational scheme for the analysis of a given set of prospective symmetry transforms $\{T_i\}$. By imposing (3) and (7), erroneous transforms can be discarded and the spectral analysis, given in (4) and (8), can be used to recover the center of rotational symmetry and the axis of the reflectional one. Moreover, based on Theorem 2, one can start with a pair of reflection transforms $\{T_{D_1}, T_{D_2}\}$ and recover the rotational transform T_{C_K}. Note that, in practice, the prospective transforms $\{T_i\}$ are computed by the spectral matching algorithm discussed in Section 4. That procedure provides an alternative geometrical approach to recovering the symmetry centers and axes. Using both approaches, we are able to cross-validate the results.

The determinant value tests of the symmetrical transforms ((3) and (7)) can be applied to higher dimensional data sets, as well as the spectral analysis in (4) and (8). The equivalent in 3D data is given by *Euler's theorem* [17].

3 Previous Work

This section overviews previous work related to our scheme. Section 3.1 provides a survey of recent results in symmetry analysis, while Section 3.2 presents the notion of Local Features that are used to represent an image as a set of salient points. A combinatorial formulation of the alignment of sets of points in R^n is discussed in Section 3.3, and a computationally efficient solution via spectral relaxation is presented. The latter approach paves the way for the proposed SSA algorithm presented in Section 4.

3.1 Previous Work in Symmetry Detection and Analysis

Symmetry has been thoroughly studied in the literature from theoretical, algorithmic, and application perspectives. Theoretical analysis of symmetry can be found in [16], [18]. The algorithmic approaches to its detection can be divided into several categories, the first of which consists of intensity-based schemes that compute numerical moments of image patches. For instance, detection of vertical reflectional symmetry using a 1D odd-even decomposition is presented in [19]. The authors assume that the symmetry axis is vertical, and thus scan each horizontal line in the image. Each such line is treated as a 1D signal that is normalized and decomposed into odd and even parts. From odd and even parts, the algorithm constructs a target function that achieves its maximum at the point of mirror symmetry of the 1D signal. When the image has a vertical symmetry axis, all symmetry points of the different horizontal lines lie along a vertical line in the image.

A method that estimates the relative rotation of two patterns using Zernike moments is suggested in [20]. This problem is closely related to the problem of detecting rotational symmetry in images. Given two patterns, where one pattern is a rotated replica of the other pattern, the Zernike moments of the two images will have the same magnitude and some phase differential. The phase differential can be used to estimate the relative rotation of the two images.

In order to detect large symmetric objects, such schemes require an exhaustive search over all potential symmetry axes and locations in the image, requiring excessive computation even for small images. An efficient search algorithm for detecting areas with high local reflectional symmetry that is based on a local symmetry operator is presented in [5]. It defines a 2D reflectional symmetry measure as a function of four parameters x, y, θ, and r, where x and y denote the center of the examined area, r is its radius, and θ is the angle of the reflection axis. Examining all possible values of x, y, r, and θ is computationally prohibitive; therefore, the algorithm formulates the search as a global optimization problem and uses a probabilistic genetic algorithm to find the optimal solution efficiently.

A different class of intensity-based algorithms [3], [7], [21] utilizes the Fourier transform to detect global symmetric patterns in images. The unitarity of the Fourier transform preserves the symmetry of images in the Fourier domain: A symmetric object in the intensity domain will also be symmetric in the Fourier domain. Derrode and Ghorbel [3] analyze the symmetries of real objects by computing the Analytic Fourier-Mellin transform (AFMT). The input image is interpolated on a polar grid in the spatial domain before computing the FFT, resulting in a polar Fourier representation. Lucchese [7] provides an elegant approach to analyzing the angular properties of an image, without computing its polar DFT. An angular histogram is computed by detecting and binning the pointwise zero crossings of the difference of the Fourier magnitude in Cartesian coordinates along rays. The histogram's maxima correspond to the direction of the zero crossing. In [21], Keller et al. extended Lucchese's work by applying the PseudoPolar Fourier transform to computing an algebraically accurate line integral in the Fourier domain. The symmetry resulted in a periodic pattern in the line integral result. This was detected by spectral analysis (MUSIC). These algorithms are by nature global, being able to effectively detect fully symmetric images, such as synthetic symmetric patterns. Yet, some of them [21] struggle at detecting small localized symmetric objects embedded in clutter.

The frequency domain was also utilized by Lee et al. in [22], where Frieze expansions were applied to the input image, thus converting planar rotational symmetries into periodic 1D signals whose period corresponds to the order of the symmetry. This period is estimated by recovering the maxima of the Fourier spectrum.

Recent work emphasizes the use of *local* image features. The local information is then agglomerated to detect the global symmetry. Reisfeld et al. [8] suggested a low-level, operator for interest points detection where symmetry is considered a cue. This symmetry operator constructs the symmetry map of the image by computing an edge map, where the magnitude and orientation of each edge depend on the symmetry associated with each of its pixels. The proposed operator is able to process different symmetry scales, enabling it to be used in multiresolution schemes.

A related approach was presented in [23], where both reflectional and rotational symmetries can be detected, even under a weak perspective projection. A Hough transform is used to derive the symmetry axes from edge contours. A refinement algorithm discards erroneous symmetry axes by imposing geometrical constraints using a voting scheme.

An approach related to our work was introduced in [24], where the symmetry is analyzed as a symmetry of a set of points. For an object, given by a sequence of points, the symmetry distance is defined as the minimum distance in which we need to move the points of the original object in order to obtain a symmetric object. This also defines the symmetry transform of an object as the symmetric object that is closest to the given one. This approach requires finding point correspondences, which is often difficult, and an exhaustive search over all potential symmetry axes is performed.

Shen et al. [9] used an affine-invariant feature vector computed over a set of interest points. The symmetry was detected by analyzing the cross-similarity matrix of this vector. Rotational and reflectional symmetries can be analyzed by finding the loci corresponding to its minima.

The gradient vector flow field was used in [25] to compute a local feature vector. For each point, its location,

orientation, and magnitude were retained. Local features in the form of Taylor coefficients of the field were computed and a hashing algorithm was then applied to detect pairs of points with symmetric fields, while a voting scheme is used to robustly identify the location of symmetry axis.

3D symmetry was analyzed in [4], [26]. The scheme computes a reflectional symmetry descriptor that measures the reflectional symmetry of 3D volumes, for all planes passing through the center of mass. The descriptor maps any 3D volume to a sphere, where each point on the sphere represents the symmetry in the object with respect to the plane perpendicular to the direction of the point. As each point on the sphere also represents the integration over the entire volume, the descriptor is resilient to noise and to small variations between objects. We show that our approach is directly applicable to 3D meshes.

SIFT local image features [13] were applied to symmetry analysis by Loy and Eklundh in [6]. In their scheme, a set of feature points is detected over the image, and the corresponding SIFT descriptors are computed. Feature points are then matched in pairs by the similarity of their SIFT descriptors. These local pairwise symmetries are then agglomerated by a Hough voting space of symmetry axes. The vote of each pair in the Hough domain is given by a weight function that measures the discrepancy in the dominant angles and scales [13] of the feature points. As the SIFT descriptors are not reflection-invariant, reflections are handled by mirroring the SIFT descriptors.

In contrast, our scheme is based on a spectral relaxation of the self-alignment problem. It recovers the self-assignment directly. Thus, we avoid the quantization of the Hough space, and our scheme can be applied, as is, to analyzing higher dimensional data and will not suffer the curse dimensionality exhibited by a density (voting) estimation scheme, such as the Hough transform. Also, our scheme does not require a local symmetry measure, such as the dominant angle, and is purely geometric. It can be applied with any local feature, such as correlators and texture descriptors [27].

The work of Hays et al. in [28] is of particular interest to us as it combines the use of local image descriptors and spectral high-order assignment for *translational symmetry* analysis. Translational symmetry is a problem in texture analysis, where one aims to identify periodic or near-regular repeating textures, commonly known as lattices. Hays et al. propose detecting translational symmetry by detecting feature points and computing a *single,* high order, spectral self-alignment. The assignments are then locally pruned and regularized using thin-plate spline warping. The corresponding motion field is elastic and nearly translational; hence, the term translational symmetry.

In contrast, our scheme deals with rotational and reflectional symmetries, where the estimated self-alignments relate to rotational motion. The core of our work is the analysis of *multiple* self-assignments and their manifestation via *multiple* eigenvectors and eigenvalues. Moreover, based on the spectral properties of geometric transform operators, we introduce a *global* assignment pruning measure, able to detect erroneous self-assignments. This comes out to be essential in analyzing symmetries in real images, which are often embedded in clutter.

(a) (b)

Fig. 2. Feature point detectors. (a) A Hessian-based scale-invariant detector is more suitable for nonstructured scenes (b) MSER responds best to structured scenes.

3.2 Local Features

The use of local features is one of the cornerstones of modern computer vision. They were found to be instrumental in a diverse set of computer vision applications such as image categorization [29], mosaicking [30], and tracking [31], to name a few. Originating from the seminal works of Schmid and Mohr [14] and Lowe [13], local features are used to represent an image I by a sparse set of salient points $\{x_i\}$, where each point is represented by a vector of parameters D_i denoted a *descriptor*. The salient set $\{x_i\}$ is detected by a *detector*.

The detector and descriptor are designed to maximize the number of interest points that will be redetected in different images of the same object and reliably matched using the descriptors. The descriptor characterizes a small image patch surrounding a pixel. Due to their locality, local features are resilient to geometrical deformations and appearance changes. For instance, a global complex geometrical deformation can be normalized locally by estimating a dominant rotation angle and characteristic scale per patch, or by estimating local affine shape moments [32]. The choice of the geometrical normalization measures depends on the geometrical deformation we aim to handle. The set of local features $\{D_i\}$ is then denoted the *image model* of a particular image.

Definition 3 (Image model). *The image model M is made of the set of N interest points $S = \{\mathbf{x}_i\}_1^N$, the corresponding set of local descriptors $\{\mathbf{D}_i\}_1^N$, and a set of local attributes $\{\theta_i, \sigma_i\}_1^N$. θ_i and σ_i are the local dominant orientation and scale, respectively, of the point i. Denote $M = \{M_i\}_1^N$, where $M_i \triangleq \{\mathbf{x}_i, \mathbf{d}_i, \theta_i, \sigma_i\}$.*

A myriad of region detectors and descriptors can be found in the literature [33], one of the most notable being Lowe's SIFT descriptor [13]. Various objects might require different combinations of local detectors and descriptors [33], depending on the object's visual properties. For instance, SIFT [13] excels in detecting and describing naturally textured images, while large piecewise constant objects are better detected by the affine covariant MSER [34], as shown in Fig. 2b. The ellipses in the figure represent the second moment matrix of the detected regions. In contrast, nonstructured objects are better characterized by affine-adapted Hessian-like detectors, as depicted in Fig. 2a.

The common solution is to use multiple descriptors simultaneously [35]. In the context of symmetry detection

(in contrast to object recognition), the local features are all extracted from the same image. Hence, one can assume that symmetric points within the same image would respond well to the same type of local detector/descriptor. This allows us to use one detector-descriptor pair at a time.

3.3 Spectral Matching of Sets of Points in R^n

Given two sets of points in $\mathbb{R}^n$ such that $S_1 = \{x_i^1\}_1^{N_1}$ and $S_2 = \{x_j^2\}_1^{N_2}$, where $x_j^k \in \mathbb{R}^n$, $k = 1, 2$, we aim to find a correspondence map $C = \{c_{i_k j_k}\}_1^{N_1}$ such that $c_{i_k j_k}$ implies that the point $x_{i_k}^1 \in S_1$ corresponds to the point $x_{j_k}^2 \in S_2$. Spectral point matching was first presented in the seminal work of Scott and Longuet-Higgins [36], who aligned point sets by performing singular value decomposition on a point association weight matrix. In this work, we follow a different formulation proposed by Berg et al. [37] and its spectral relaxation introduced by Leordeanu and Hebert in [12]. We start by formulating a binary quadratic optimization problem, where the binary vector $Y \in \{0, 1\}$, represents all possible assignments of a point $x_{i_k}^1 \in S_1$ to the points in set S_2. The assignment problem is then given by

$$Y^* = \arg\max_Y \{Y^T H Y\}, \quad Y \in \{0, 1\}, \tag{11}$$

where H is an affinity matrix such that $H(k_1, k_1)$ is the affinity between the matchings $c_{i_{k_1} j_{k_1}}$ and $c_{i_{k_2} j_{k_2}}$. $H(k_1, k_1) \to 1$ implies that both matchings are consistent, and $H(k_1, k_1) \to 0$ implies that the matchings are contradictory. In practice we use

$$H(k_1, k_1) = \exp\left(-\frac{1}{\sigma}\left(d\left(x_{i_{k_1}}^1, x_{i_{k_2}}^1\right) - d\left(x_{j_{k_1}}^2, x_{j_{k_2}}^2\right)\right)^2\right), \tag{12}$$

where σ is a scale factor. This binary quadratic optimization is known to be *np*-hard [38], and its solution can be approximated by spectral relaxation

$$Z^* = \arg\max_Z \frac{Z^T H Z}{Z^T Z}, \quad Z \in \mathbb{R}. \tag{13}$$

Thus, Z^* is given by the eigenvector corresponding to the largest eigenvalue λ_1, as this maximizes (13). This approach can be considered as normalized cut clustering applied to the set of correspondences $\{c_{i_k j_k}\}_1^{N_1 N_2}$. Namely, we assume that the true correspondences $\{c_{i_k j_k}\}_1^M$ ($M \ll N_1 N_2$) form a tightly connected cluster based on the affinity measure in (12). In [39], Cour et al. proposed a doubly-stochastic normalization of the affinity matrix H by adding an affinity constraint over the solution Z to enforce one-to-one matchings.

Given the relaxed solution Z^*, we apply the discretization procedure given in [12] to derive an approximation $\widehat{Y}$ to the binary vector Y^*. Note that since we are interested in symmetry analysis, we expect to recover multiple solutions (eigenvectors) $\{\widehat{Y}_i\}_1^K$, where K is the order of symmetry. In the following section, we show how to estimate K based on the eigenvalues of the affinity matrix H and how to recover the symmetry correspondences. We then compute the symmetry centers for rotational symmetry, and axes of reflection for reflectional symmetry.

4 Spectral Symmetry Analysis

In this section, we apply spectral matching to symmetry analysis and derive the spectral symmetry analysis scheme.

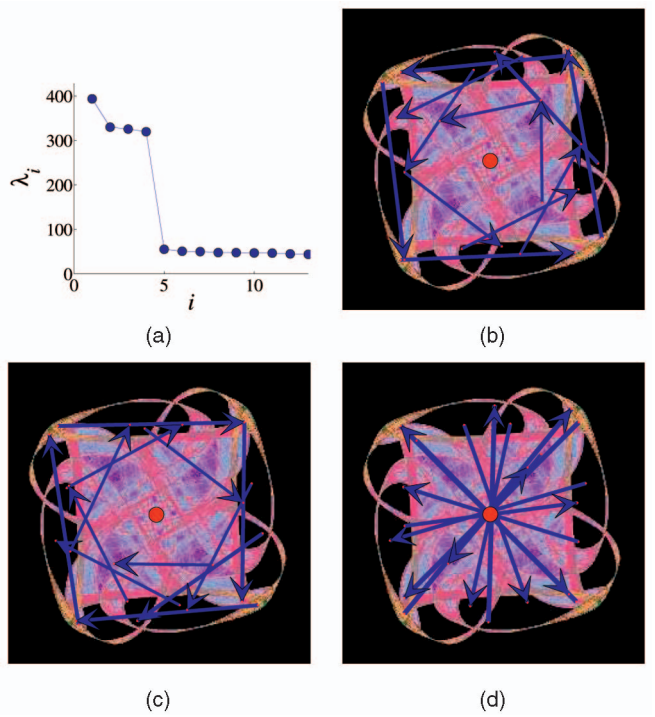

Fig. 3. Rotational symmetry. (a) Eigenvalues λ_i. (b) The rotation corresponding to λ_2. (c) The rotation corresponding to λ_3. (d) The rotation corresponding to λ_4.

We start in Section 4.1, by presenting a general computational approach for the detection and analysis of symmetries of sets of points in n-dimensional spaces. We then elaborate on the analysis of symmetry in 2D images in Section 4.2.

4.1 Spectral Symmetry Analysis of Sets in $\mathbb{R}^n$

Given a set of points $S \in \mathbb{R}^n$, with a symmetry of order K. It follows by Section 2 that there exists a set of symmetry transformations $\{T_{C_K}\}$ and $\{T_{D_K}\}$ that maps S to itself. The main issue is how to detect these multiple transformations simultaneously. In terms of numerical implementation, this implies that one has to look for a set of local solutions of the corresponding optimization problem. Most matching and alignment schemes, such as RANSAC and ICP, lock on to a *single* optimal alignment, and it is unclear how to modify them to search for multiple solutions.

Spectral relaxation provides an elegant solution to this issue. The multiple self-alignments will be manifested by the multiple maxima of the binary formulation in (11) and its corresponding relaxation in (13). The maxima of the Reighley quotient in (13) are the leading eigenvalues of the affinity matrix H, and the corresponding arguments are the corresponding eigenvectors. This beautiful property allows us to recover multiple assignments simultaneously and independently by computing the eigendecomposition of H.

Such an example is given in Fig. 3, where the four self-alignments are manifested by four dominant eigenvalues. Note that the largest eigenvalue corresponds to the identity transform that maps each point to itself. Hence, given the set of interest points $S \in \mathbb{R}^n$, we apply the spectral alignment algorithm in Section 3.3 and compute the eigendecomposition $\{\psi_i, \lambda_i\}_1^K$ of (13). The overall number of symmetry axes is given by the number of large eigenvalues K, and the correspondence maps $\{C_i\}_1^K$ are derived by the discretized binary eigenvectors $\{\psi_i\}$.

As the spectral alignment matches euclidean distances between points, it can be used to compute multiple nonparametric alignments. This implies that we do not have to predefine which symmetry type to analyze; those that do exist will be detected. However, this also implies that the scheme might detect erroneous self-alignments, which are unrelated to symmetry. This phenomenon would become evident during the analysis of symmetric sets embedded in clutter. The problem is resolved in the next section by incorporating the geometrical constraints of the symmetry transforms discussed in Section 2. This allows us to prune the erroneous self-alignments.

4.1.1 Perfect Symmetry and Spectral Degeneracy

When analyzing perfectly symmetric sets of points, multiple alignments might be manifested by the same eigenvalue and the corresponding eigenvector becomes degenerate. Each eigenvector is then a linear combination of several assignments.

This phenomenon *never* occurs with data sources other than synthetic sets of points. For instance, in images the feature point detectors have a certain subpixel accuracy and corresponding feature points do not create perfect symmetries. This applies to synthetic images and even more so to real images and 3D objects that are never perfectly symmetric.

In order to generalize our approach to perfectly symmetric sets of points, we propose adding Gaussian random noise $N(0, \sigma_n^2)$ to the nonzero elements of the affinity matrix. This breaks down the perfect symmetry, if it exists, and does not influence the analysis of regular data. In order to retain the symmetricity of the affinity matrix, we add a symmetric pattern of noise. As the nonzero affinities are of $O(10^{-1})$ for a well-chosen value of σ in (12), we used $\sigma_n = 10^{-3}$.

4.2 Spectral Symmetry Analysis of Images

An image $I \in \mathbb{R}^2$ is a scalar or vector function defined over $\mathbb{R}^2$. As such, the spectral matching scheme cannot be used, as it applies to sets of points. Hence, we turn to image modeling by means of local features, as discussed in Section 3.2. This allows us to represent the input image as a set of salient points. The rotation invariance of the detectors guarantees that corresponding symmetric points would be detected as salient points simultaneously. We then present in Section 4.2.2 a scheme for pruning erroneous spectral alignments and identifying valid matchings as C_K or D_K. Last, given the pruned valid transforms, we show in Section 4.2.3 how to recover the intrinsic geometrical properties (center of rotation and axis of reflection for C_K or D_K, respectively) of each detected symmetry.

4.2.1 Image Representation by Local Features

Given an input image I, we compute an image model M for each type of local detector/descriptor. A reflected replica of the features is then added to M [6]. This allows us to handle reflections, recalling that the local features are rotationally but not reflectionally-invariant. The features are then progressively sampled [40] to reduce their number to a few thousand. The progressive sampling spreads the points evenly over the image, thus reducing the number of image regions with high numbers of features. These are prone to producing local partial matches.

We also utilize the dominant-scale property of the local features [13] to prune false pairwise assignments and further sparsify the affinity matrix H. As we analyze self-alignments within the same image, corresponding features will have similar dominant scales. Hence, we discard point-to-point matches whose ratio of local scales is more than a predefined threshold, and set the corresponding pairwise affinities in (12) to zero.

In order to effectively utilize the sparsity of the affinity matrix H, we threshold it by $T = 10^{-5}$. Namely, the affinity in (12) is always nonzero. But, in practice, for geometrically inconsistent pairs, the affinity is of $O(10^{-7})$, while the consistent pairs are of $O(10^{-1})$.

4.2.2 Symmetry Categorization and Pruning

Given the image model M, we apply the spectral matching scheme described in Section 3.3, and derive P tentative self-alignments of the image denoted $\{C_i\}_1^P$. Typically $P \gg K$, K being a typical order of image symmetry. In practice, $K < 10$ and $P \approx 15$, the reason being that, in real images, the symmetric patterns might be embedded in clutter, resulting in the recovery of spurious self-alignments (eigenvectors) unrelated to the symmetry.

To address this issue, we propose an assignment pruning scheme that is based on the determinant value property of symmetry transforms in $\mathbb{R}^2$. Namely, by computing the projective transform corresponding to the recovered matching, and recalling that the determinant of a symmetry transform is ± 1 (Section 2), erroneous matchings can be pruned. Moreover, this provides a mean for categorizing transforms to either C_K or D_K.

We analyze each correspondence map C_i by applying a normalized DLT algorithm [41] and fitting a projective motion model T_i:

$$T_i X_1 = X_2 = \begin{bmatrix} t_{11} & t_{12} & t_{13} \\ t_{21} & t_{22} & t_{23} \\ t_{31} & t_{32} & 1 \end{bmatrix} \begin{bmatrix} x_1 \\ y_1 \\ 1 \end{bmatrix} = \begin{bmatrix} x_2 \\ y_2 \\ 1 \end{bmatrix}, \qquad (14)$$

X_1 and X_2 being the spatial coordinates of corresponding points in C_i.

Equation (14) can also be solved for an affine motion model, where the choice of the model (projective versus affine) depends on the expected distortion within the image. The correspondence map C_i can be pruned for erroneous point matchings by applying a robust Least-Squares scheme, such as RANSAC [42].

Given the transform T_i, we can now apply (3) and (7) and classify a transform T_i as a cyclic symmetry C_K if $\det(T_i) \approx 1$, a reflectional symmetry D_K if $\det(T_i) \approx -1$, or discard it as an erroneous self-alignment otherwise. Algorithm 1 summarizes the first two steps of the SSA.

Algorithm 1. Spectral Symmetry Analysis of Image

1: Create an image model M of the input image. Suppose it contains N points.
2: Set P, the number of eigenvectors to analyze and ε, the determinant value error of the symmetry transform.
3: Progressively sample the interest regions.
4: Reflect all the local descriptors $\{\mathbf{D}_i\}_1^N$ in the image while preserving the originals.
5: Compute an affinity matrix based on putative correspondences drawn by similar descriptors $\{\mathbf{D}_i\}_1^N$ and the dominant-scale pruning measure.

6: Add random noise to the affinity matrix.
7: Solve (13) and compute the eigendecomposition $\{\psi_i, \lambda_i\}$.
8: **while** $i < P$ **do**
9: Derive correspondence map C_i from ψ_i
10: Estimate transformation matrix T_i
11: **if** $|\det(T_i) - 1| < \varepsilon$ **then**
12: Rotation detected—use (4) to find the center
13: **else if** $|\det(T_i) + 1| < \varepsilon$ **then**
14: Reflection detected—use (8) to find the reflection axis
15: **end if**
16: **end while**

We emphasize that the spectral matching and pruning schemes can also be applied to sets of points in higher dimensions. An example of symmetry analysis of a 3D object is provided in Section 5.

4.2.3 Computing the Geometrical Properties of the Symmetry

The center of symmetry and axis of rotation can be computed by complementary *geometrical* and *analytical* approaches. The axis of reflection can be computed analytically, given the corresponding transform T_{D_K}, by applying (8). The reflection axis is the line connecting the two points, corresponding to the two eigenvectors of T_{D_K} with an eigenvalue of $\lambda_i = 1$. We denote this the *analytical* solution. In addition, one can apply a *geometrical* solution, where we connect the corresponding points in D_K found by spectral matching. These are the points which were used to estimate T_{D_K} in the previous section. The reflection axis is the line that fits through the middle point of each such line segment.

Given the transform T_{C_K}, corresponding to some rotational symmetry C_K, the center of rotation can be recovered by applying (4) and computing the eigenvector of T_{C_K}, corresponding to $\lambda_i = 1$. The center of rotation can also be computed *geometrically* by connecting matching points. For each such line, consider the normal passing through its middle, as all such normals intersect at the center of rotation. Thus, the center of rotation is derived by solving an overdetermined set of equations in the least-squares sense, similar to the robust fitting of the reflection axes.

Theorems 1 and 2 provide the foundation for inferring the complete set of symmetries, given a subset of them, detected by spectral analysis. Given two reflectional symmetry transforms $\{D_{K_1}, D_{K_2}\}$, the order of symmetry can be derived by computing the angle between the reflection axes $\Delta\alpha$. The order of symmetry is then given by solving

$$\frac{2\pi}{\Delta\alpha} Z = K, \quad Z, K \in \mathbb{Z}.$$

For instance, given two reflectional axes with a relative angle $\Delta\alpha = \frac{\pi}{2}$ implies that the object has at least two reflectional symmetry axes. But there might also be four or even eight symmetry axes. That would imply that the spectral scheme identified only a subset of the axes.

Hence, the symmetry order can be estimated up to scale factor Z. Given more than two reflection axes, one can form a set of equations over the integer variables $\{Z_i\}$

$$\begin{aligned} \frac{2\pi}{\Delta\alpha_1} Z_1 &= K, \\ &\vdots \\ \frac{2\pi}{\Delta\alpha_n} Z_n &= K. \end{aligned} \tag{15}$$

As $K < 8$ for most natural objects, (15) can be solved by iterating over $K = 1 \ldots 8$ and looking for the value of K for which all of the $\{Z_i\}$ are integers.

5 Experimental Results

In this section, we experimentally verify the proposed Spectral Symmetry Analysis scheme by applying it to real images and volumes. In Section 5.1 we apply the SSA to a set of real images, where the detection of the symmetries becomes increasingly difficult. This allows us to exemplify the different aspects of the SSA, as the simple examples point out the core of the SSA, and the more difficult ones require the more elaborate components. In Section 5.2, we apply our scheme to the BioID face database [43]. This data set consists of 1,521 face images with ground truth symmetry axes. This allows to asses the scheme's accuracy and compare it to Loy and Eklundh [6], whose results are considered state of the art. Last, we detect symmetries in 3D objects in Section 5.3.

5.1 Symmetry Analysis of Images

Fig. 3 presents the analysis of a synthetic image with rotational symmetry of order four. Applying Algorithm 1 produces the sets of corresponding eigenvalues and eigenvectors λ_i and ψ_i, respectively. The spectral gap in Fig. 3a is evident and allows us to estimate the order of symmetry. Note that the different self-alignments are manifested by nonequal eigenvalues, despite the image being synthetic. We attribute that to the imperfectness of the feature point detectors, detecting the feature points at slightly different locations, and to the addition of noise to the feature point coordinates. The transformation T_{C_1}, corresponding to the leading eigenvalue λ_1, is found to correspond to the identity transform and is thus discarded. By estimating T_{C_2}, the symmetry is found to be a rotational symmetry as $\det(T_{C_2}) \approx 1$. Applying (4) to T_{C_2} recovers the center of symmetry that is marked by a red dot in Fig. 3b. Eigenvalues λ_3, λ_4 uncover the remaining symmetrical self-alignments, which are drawn in Figs. 3c and 3d, respectively. The analysis of $\{\lambda_i\}_{i>4, i<P}$ reveals that the remaining alignments are either identity transforms or repetitions of previously found symmetries. Such duplications are identified and discarded using the Frobenius norm.

Fig. 4 depicts an object with a reflectional symmetry. The eigenvalues shown in Fig. 4a indicate that besides the trivial identity transform represented by λ_1, there exists an alternative self-alignment. This point correspondence, derived from ψ_2, is shown in Fig. 4b, and by computing $\det(T_{C_2}) \approx -1$, we conclude that it is a reflectional symmetry. The symmetry axis is then recovered by applying (8) to T_{C_2} and connecting the two eigenvectors corresponding to $\lambda_i = 1$. Similar results are achieved by fitting the normal line to middle of the line segments connecting the corresponding points. The resulting reflection axis is shown in Fig. 4b.

Fig. 5 presents an image exhibiting both rotational and reflectional symmetries, and the SSA is able to detect both

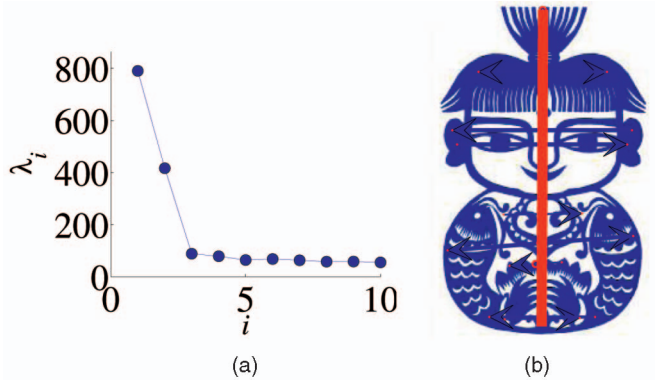

Fig. 4. Reflectional symmetry. (a) Eigenvalues λ_i. (b) The reflection corresponding to λ_2.

simultaneously. The corresponding eigenvalues reported in Fig. 5a reveal the existence of three nontrivial self-alignments due to the four leading eigenvalues. We proceed by computing the corresponding transformations T_{C_2}, T_{C_3}, and T_{C_4}. T_{C_2} and T_{C_3} come out to be the reflectional symmetries presented in Figs. 5b and 5c, along with the reflection axis marked by a red line. The third nontrivial self-correspondence T_{C_4} is detected as a rotation, as $\det(T_{C_4}) \approx 1$. C_4 , and the corresponding mapping and the estimated rotation center are depicted in Fig. 5d.

Fig. 6 presents an example of a real image, where the distinctiveness of the eigenvalues corresponding to symmetric patterns degrades due to the image properties. Those include poor image quality and appearance variations of the corresponding symmetric parts, which cannot be compensated by the local features. Most of the interest points lie within the background, creating a highly cluttered set of points, as can be seen in Fig. 6b. We analyzed the $P = 15$ eigenvectors corresponding to the P leading eigenvalues and applied the determinant value test to the corresponding transforms $\{T_{C_i}\}_1^P$. The determinant values $\{\det(T_{C_i})\}_1^P$ are depicted in Fig. 6a and reveal that only T_{C_1} and T_{C_2}

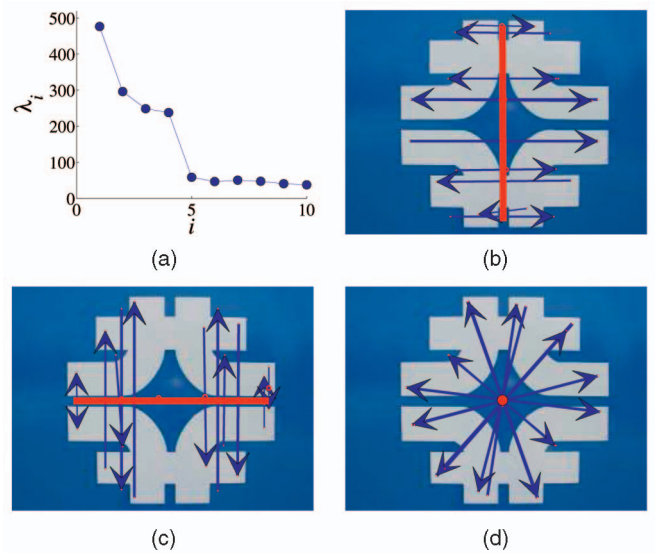

Fig. 5. Rotational and reflectional symmetries. (a) The eigenvalues λ_i. (b) The symmetric transform corresponding to λ_2. (c) The symmetric transform corresponding to λ_3. (d) The symmetric transform corresponding to λ_4.

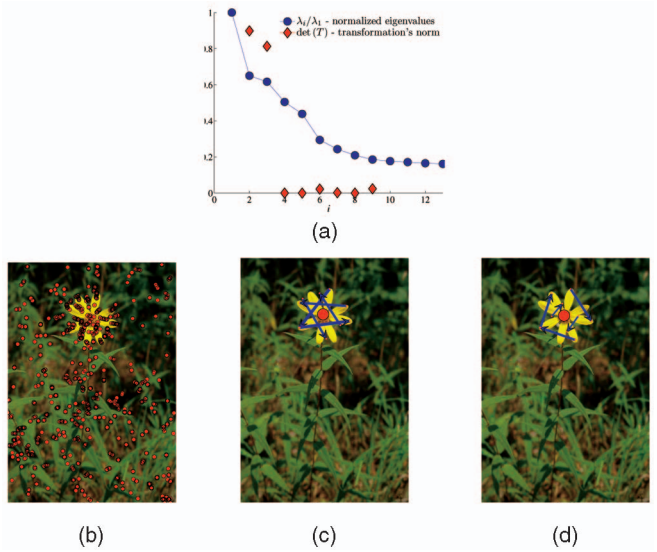

Fig. 6. Symmetric pattern embedded in clutter. (a) Eigenvalues λ_i. (b) Interest points, in both object and (mostly) background. (c) Symmetric transform corresponding to ψ_2. (d) Symmetric transform corresponding to ψ_3.

correspond to symmetries, while the other transformations are pruned. As both $\det(T_{C_1})$ and $\det(T_{C_2})$ are close to 1, both are rotations. The corresponding point alignments and rotation centers are shown in Figs. 6c and 6d.

Fig. 7 takes us further with a real-life object, where, despite the object being both rotationally and reflectionally symmetric, only reflectional symmetries are detected, due to the lack of appropriate local descriptors. The detected reflectional alignments corresponding to the three largest eigenvalues are shown in Figs. 7b, 7c, 7d, and 7e. Examining $\{T_{C_i}\}_{i=4}^{15}$ does not reveal the expected rotational symmetry transforms. Examining the image it is evident that the geometrically corresponding points show dissimilar intensities. Namely, the SSA was able to detect *pseudosymmetry*, a pattern of geometrical symmetry lacking the corresponding intensity symmetry. This property is intriguing, as most human viewers would indeed consider

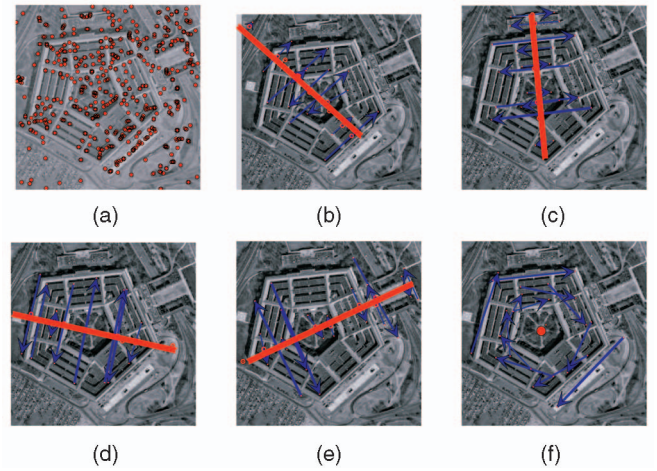

Fig. 7. Inferring rotational symmetry from multiple reflections. (a) Interest points. (b) Reflection corresponding to ψ_2. (c) Reflection corresponding to ψ_3. (c) Reflection corresponding to ψ_4. (e) Reflection corresponding to ψ_5. (f) Rotational symmetry inferred from the reflections.

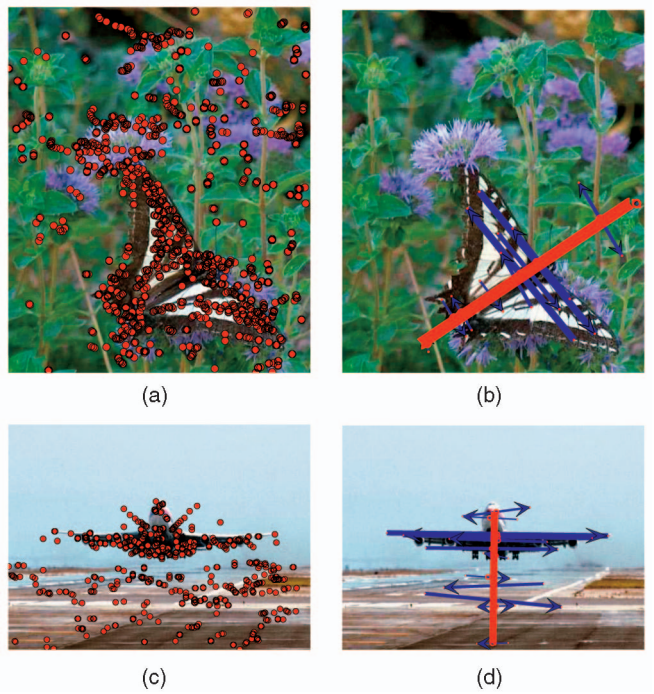

Fig. 8. Reflectional symmetry embedded in clutter.

the Pentagon a symmetric object. By applying Theorem 2, we are able to infer the rotational symmetry based on the detected reflections.

Fig. 8 demonstrates successful symmetry detection in the presence of heavily cluttered background by applying the transformation pruning measure. Fig. 9 is another example (as the Pentagon in Fig. 7) of a *pseudosymmetric* object whose symmetry is far from being perfect and can be argued by some. Background clutter and low repeatability of interest regions challenge the symmetry detection

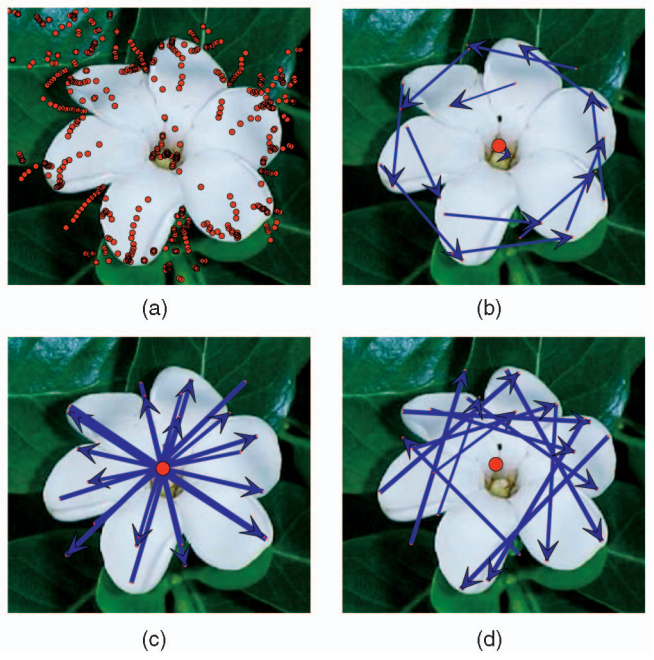

Fig. 9. Rotational near-symmetry with clutter and low repeatability of interest regions.

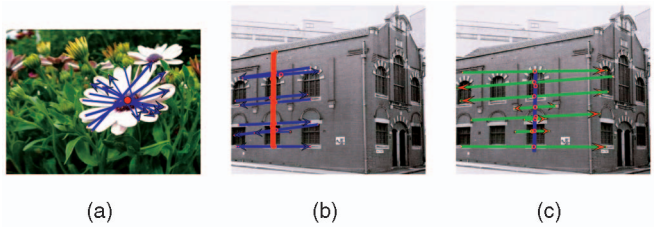

Fig. 10. (a) Rotation detection under affine distortion. (b) Reflection detection under affine distortion. (c) Failed symmetry detection. The corresponding points are not symmetrical in the real world but only within the image.

algorithm further. Still, the SSA manages to come out with three rotational symmetries, as can be seen in Figs. 9b, 9c, and 9d. Fig. 10c presents an image where the SSA detected a false symmetry, along with correctly detected local symmetry, which is shown in Fig 10b. In this image, our underlying assumption that symmetries are manifested by multiple self-alignments is invalid due to the projection of the 3D object onto the 2D plane of the camera.

Fig. 11 depicts more results of the SSA. Symmetry detection of faces is shown in Figs. 11a, 11b, 11c, and 11d. This is of particular interest as face features are inherently symmetric and there are numerous works [44] aimed at their detection without explicitly utilizing symmetry. Note that SIFT features are able to capture corresponding symmetric features, but not those considered important in face recognition, such as the mouth tips and the nostrils. In Fig. 11h, a false symmetric correspondence is detected alongside the true symmetry in the car's wheel. It could have been discarded by requiring that points along a symmetry axes will also be part of a rotational symmetry, as reflectional symmetry is always accompanied by rotational symmetry (see Section 2). Also, we did not impose a size

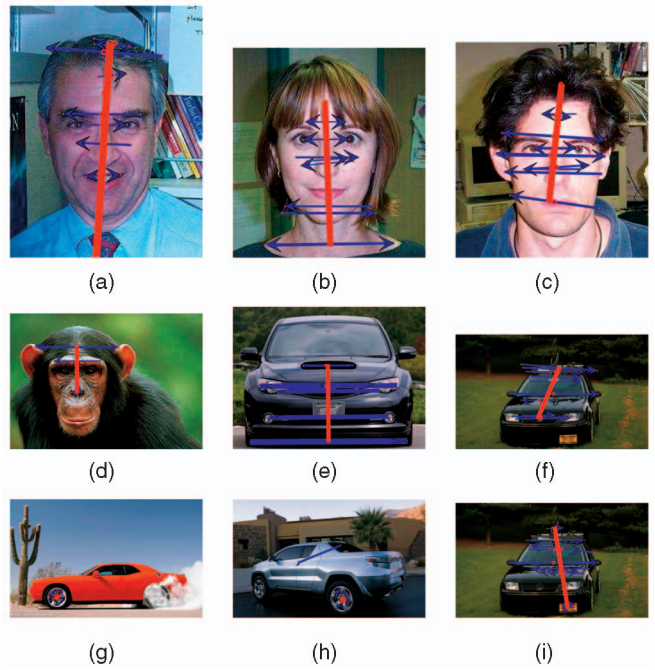

Fig. 11. (a)-(i) Symmetry analysis results. (b)-(d) are taken from the Caltech 256 database. In (h), we notice a spurious correspondence having the same reflection axis as the true symmetry. The SSA fails in (i) due to the detection of erroneous feature points.

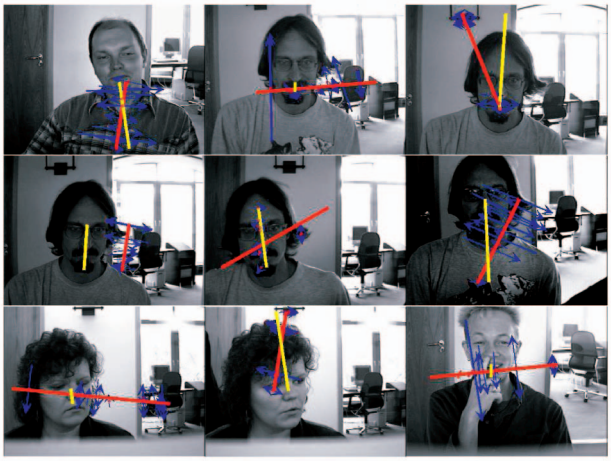

Fig. 12. All of the images from the BioID data set consisting of 1,521 images for which the symmetry analysis failed. The ground truth symmetry axes are annotated in yellow, while the detected axes are annotated in red.

Fig. 13. Some of the images from the BioID data set, consisting of 1,521 images, for which the symmetry analysis was successful. We achieved an accuracy rate of 99.41 percent. The ground truth symmetry axes are annotated in yellow, while the detected axes are annotated in red.

constraint on the detected symmetric object or its aspect ratio. This exemplifies that, in real applications, one can add task-specific geometrical constraints and improve the results. Fig. 11h shows another failure of the SSA, where a false symmetry axis is detected. Note that a valid axis was detected in the same image in Fig. 11f. The failure is due to the detection of spurious feature points on the car's hood.

5.2 Statistical Accuracy Analysis

In order to assess the SSA's accuracy and compare it to previous results over an image data set of substantial size, it was applied to detect the axes of symmetry in 1,521 images from the BioID face database [43]. This data set was used by Loy and Eklundh [6] and we follow their experiential setup. This data set also contains the locations of 20 facial feature points (eyes, mouth tips, etc.) manually annotated in each image. Those points are used to compute the ground truth symmetry axes. As in [6], the axis of facial symmetry was considered detected if its (r, θ) parameters were within ± 5 pixels and $\pm 5^\circ$ of the ground truth, respectively. We used 600 local features with four nearest neighbors sampled progressively out of 1,500 local features, created by a Hessian affine-invariant detector and SIFT descriptors. We achieved an accuracy of **99.41 percent** that corresponds to having only **nine misdetected** symmetry axes. Those are depicted in Fig. 12. In those images, the face area is characterized by an insufficient number of feature points due to its low contrast compared to the background. Some successful detection examples are shown in Fig. 13, while the rest of the face images with the detected symmetry axes are depicted in the supplemental materials, which can be found on the Computer Society Digital Library at http://doi.ieeecomputersociety.org/10.1109/TPAMI.2009.121.

Loy and Eklundh [6] report an accuracy of 95.1 percent, where they detected up to *five* symmetry axes per image and considered the symmetry analysis successful if *anyone* of those was accurate. To emphasize the applicability of our scheme, we only detected a *single* reflection axis, and applied the generic formulation detailed in Section 4.2. Further accuracy could have been derived by recalling that the symmetry of faces is strictly reflectional. Hence, we can tune the SSA to detect only reflectional symmetries by allowing a feature point to be matched only to descriptors of reflected feature points. Recall that in Section 4.2.1, we added those reflected feature points as image descriptors (SIFTs in this example) are not reflection-invariant. In practice, the symmetry analysis acts as an interest point detector of face-specific features, as those are symmetric.

5.3 Analysis of 3D Symmetry

The SSA can be readily applied to 3D objects. For instance, applying it to mesh objects would entail the use of the equivalent of local features in meshes. While it is clearly feasible, it is beyond the scope of this work, and we restrict the discussion to the analysis of a symmetric mesh object without any mesh-oriented local features. As such, we analyze the mesh in Fig. 14, which depicts a rectangular structure with a longer side along the Y axis. We use all vertices and build a fully connected weighted graph and affinity matrix. The eigenvalues are shown in Fig. 14a,

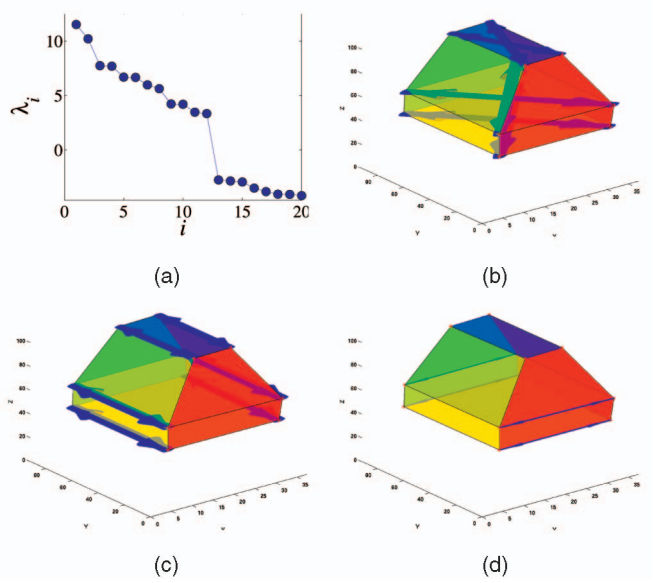

Fig. 14. The 3D symmetry. (a) The spectral alignment eigenvalues. (b) Self-correspondence by λ_2—rotation (c) Self-correspondence by λ_3—reflection (d) Self-correspondence by λ_4—reflection.

revealing four self-alignments. The first, corresponding to λ_1, is the identity transform, while the alignment derived from ψ_2 is shown in Fig. 14b and conveys a 180 degree rotation of the whole object in parallel to the $X-Y$ plane, about the base of the object. The SSA recovers two additional reflectional symmetries, corresponding to ψ_3 and ψ_4. Those are depicted in Figs. 14c and 14d. The plane of reflection is drawn in blue and intersects the object.

5.4 Implementation Issues

The SSA algorithm is fast, spending most of its time descriptors for the local features and computing the eigendecomposition of the affinity matrix H. For images with thousands of local descriptors, the affinity matrix can reach a size of $20{,}000 \times 20{,}000$, but since local appearance information is applied to reject nonpossible correspondences in advance, the affinity matrix is very sparse, $\sim$99 percent. The sparseness of the affinity matrix alleviates both the memory requirements and the computational complexity of the eigendecomposition. We implemented the SSA in Matlab and computed the local descriptors using the precompiled binary compute_descriptors made available courtesy of the VGG group. Typical running times on an Intel(R) Core(TM)2 Duo running at 2.20 GHz with 4 GB of memory are below 1 s, for creating the local descriptors, and less than 2 s for computing the eigendecomposition using Matlab's built-in eigs function.

6 Conclusions

We presented a computational scheme for the detection of symmetric structures in n-dimensional spaces. Our approach is based on the properties of the spectral relaxation of the self-alignment problem. We showed that both reflectional and rotational symmetries can be efficiently recovered by analyzing the spectral properties of this formulation. Geometrical constraints were incorporated to improve the robustness of our scheme. We applied this approach to the analysis of image by using local feature representations. The resulting scheme was shown experimentally to be both efficient and robust as we are able to detect symmetric structure embedded in clutter in real images.

Appendix

Theorem 3. *Given two distinct reflectional transforms T_{D_1} and T_{D_2}, one can recover the corresponding symmetrical rotational transforms T_{C_K}:*

$$T_{C_K} = T_{D_1} \cdot T_{D_2}. \tag{16}$$

Proof. Given a set S with two reflectional symmetry axes. The center of the corresponding rotational symmetry is at $\mathbf{c}_0 = (x_0, y_0)$ and the axis of one of the reflection axes is at an angle of α_o. Then, a reflection transform T_{D_K} is given by

$$\begin{aligned} T_{D_k}(\mathbf{c}_0, \alpha_o) = T(\mathbf{c}_0) Rot\left(-\frac{2\pi}{N}k - \alpha_o\right) \\ Ref(\widehat{y}) Rot\left(\frac{2\pi}{N}k + \alpha_o\right) T(-\mathbf{c}_0), k \in \mathbb{Z}, \end{aligned} \tag{17}$$

where $T(\mathbf{c}_0)$ is a translation by $\mathbf{c}_0$, $Rot(\alpha)$ is a rotation by α about the origin of axes, and $Ref(\widehat{y})$ is a reflection about the y axis.

Equation (17) corresponds to shifting the center of symmetry to the origin of axes, aligning the reflection axis with the Z axis, reflecting the set S about the axis Z, and inverting the rotation and translation.

Given two reflectional transforms, we get

$$\begin{aligned} &T_{D_{k_1}}(\mathbf{c}_0, \alpha_o) T_{D_{k_2}}(\mathbf{c}_0, \alpha_o) \\ &= T(\mathbf{c}_0) Rot\left(-\frac{2\pi}{N}k_1 - \alpha_o\right) Ref(\widehat{y}) Rot\left(\frac{2\pi}{N}k_1 + \alpha_o\right) T(-\mathbf{c}_0) \cdot \\ &\quad T(\mathbf{c}_0) Rot\left(-\frac{2\pi}{N}k_2 - \alpha_o\right) Ref(\widehat{y}) Rot\left(\frac{2\pi}{N}k_2 + \alpha_o\right) T(-\mathbf{c}_0) \\ &= T(\mathbf{c}_0) Rot\left(-\frac{2\pi}{N}k_1 - \alpha_o\right) Ref(\widehat{y}) \cdot \\ &\quad \underbrace{Rot\left(\frac{2\pi}{N}k_1 + \alpha_o\right) Rot\left(-\frac{2\pi}{N}k_2 - \alpha_o\right)}_{Rot\left(\frac{2\pi}{N}(k_1 - k_2)\right)} \cdot \\ &\quad Ref(\widehat{y}) Rot\left(\frac{2\pi}{N}k_2 + \alpha_o\right) T(-\mathbf{c}_0) \\ &= T(\mathbf{c}_0) Rot\left(-\frac{2\pi}{N}k_1 - \alpha_o\right) \cdot \\ &\quad \underbrace{Ref(\widehat{y}) Rot\left(\frac{2\pi}{N}(k_1 - k_2)\right) Ref(\widehat{y})}_{Rot\left(-\frac{2\pi}{N}(k_1 - k_2)\right)} \cdot \\ &\quad Rot\left(\frac{2\pi}{N}k_2 + \alpha_o\right) T(\mathbf{c}_0) = T(\mathbf{c}_0) \cdot \\ &\quad \underbrace{Rot\left(-\frac{2\pi}{N}k_1 - \alpha_o\right) Rot\left(-\frac{2\pi}{N}(k_1 - k_2)\right) Rot\left(\frac{2\pi}{N}k_2 + \alpha_o\right)}_{Rot\left(\frac{2\pi}{N}2(k_2 - k_1)\right)} \cdot \\ &\quad T(\mathbf{c}_0) = T(\mathbf{c}_0) Rot\left(\frac{2\pi}{N}2(k_2 - k_1)\right) T(-\mathbf{c}_0) \\ &\quad = Rot\left(\mathbf{c}_0, \frac{4\pi}{N}(k_2 - k_1)\right). \end{aligned}$$

$Rot(\mathbf{c}_0, \frac{4\pi}{N}(k_2 - k_1))$ is a rotation by $\frac{4\pi}{N}(k_2 - k_1)$ about the center of symmetry, and as $k_1, k_2 \in \mathbb{Z}$, it corresponds to C_K and

$$T_{C_K} = Rot\left(\mathbf{c}_0, \frac{4\pi}{N}(k_2 - k_1)\right) = T_{D_1} \cdot T_{D_2}. \tag{18}$$

□

Acknowledgments

The authors of this paper would like to thank authors of [11], for making their test data set of symmetric images public. They would also like to thank the reviewers and associate editor for their helpful and informative remarks.

References

[1] M.A. Arbib, *The Handbook of Brain Theory and Neural Networks.* MIT Press, 1995.

[2] H. Cornelius, M. Perdoch, J. Matas, and G. Loy, "Efficient Symmetry Detection Using Local Affine Frames," *Proc. 15th Scandinavian Conf. Image Analysis,* pp. 152-161, June 2007.

[3] S. Derrode and F. Ghorbel, "Shape Analysis and Symmetry Detection in Gray-Level Objects Using the Analytical Fourier-Mellin Representation," *Signal Processing,* vol. 84, no. 1, pp. 25-39, Jan. 2004.
[4] M.M. Kazhdan, B. Chazelle, D.P. Dobkin, A. Finkelstein, and T.A. Funkhouser, "A Reflective Symmetry Descriptor," *Proc. Seventh European Conf. Computer Vision—Part II,* pp. 642-656, 2002.
[5] N. Kiryati and Y. Gofman, "Detecting Symmetry in Grey Level Images: The Global Optimization Approach," *Int'l J. Computer Vision,* vol. 29, no. 1, pp. 29-45, Aug. 1998.
[6] G. Loy and J.-O. Eklundh, "Detecting Symmetry and Symmetric Constellations of Features," *Proc. European Conf. Computer Vision,* pp. 508-521, May 2006.
[7] L. Lucchese, "Frequency Domain Classification of Cyclic and Dihedral Symmetries of Finite 2D Patterns," *Pattern Recognition,* vol. 37, pp. 2263-2280, 2004.
[8] D. Reisfeld, H. Wolfson, and Y. Yeshurun, "Context Free Attentional Operators: The Generalized Symmetry Transform," *Int'l J. Computer Vision,* pp. 119-130, 1995.
[9] D. Shen, H. Ip, and E.K. Teoh, "Robust Detection of Skewed Symmetries by Combining Local and Semi-Local Affine Invariants," *Pattern Recognition,* vol. 34, no. 7, pp. 1417-1428, 2001.
[10] L. Shiv Naga Prasad and V. Davis, "Detecting Rotational Symmetries," *Proc. 10th IEEE Int'l Conf. Computer Vision,* vol. 2, pp. 954-961, Oct. 2005.
[11] M. Park, S. Lee, P.-C. Chen, S. Kashyap, A.A. Butt, and Y. Liu, "Performance Evaluation of State-of-the-Art Discrete Symmetry Detection Algorithms," *Proc. Computer Vision and Pattern Recognition Conf.,* June 2008.
[12] M. Leordeanu and M. Hebert, "A Spectral Technique for Correspondence Problems Using Pairwise Constraints," *Proc. Int'l Conf. Computer Vision,* vol. 2, pp. 1482-1489, Oct. 2005.
[13] D. Lowe, "Distinctive Image Features from Scale-Invariant Keypoints," *Int'l J. Computer Vision,* vol. 20, pp. 91-110, 2003.
[14] C. Schmid and R. Mohr, "Local Grayvalue Invariants for Image Retrieval," *IEEE Trans. Pattern Analysis and Machine Intelligence,* vol. 19, no. 5, pp. 530-535, May 1997.
[15] H.S.M. Coxeter, *Introduction to Geometry.* John Wiley & Sons, 1969.
[16] H. Weyl, *Symmetry.* Princeton Univ. Press, 1952.
[17] E. Trucco and A. Verri, *Introductory Techniques for 3D Computer Vision,* pp. 333-334. Prentice-Hall, 1998.
[18] W. Miller, *Symmetry Groups and Their Applications.* Academic Press, 1972.
[19] S. Chen, "Extraction of Local Mirror-Symmetric Feature by Odd-Even Decomposition," *Proc. Int'l Conf. Image Processing,* vol. 3, pp. 756-759, 2001.
[20] W. Kim and Y. Kim, "Robust Rotation Angle Estimator," *IEEE Trans. Pattern Analysis and Machine Intelligence,* vol. 21, no. 8, pp. 768-773, Aug. 1999.
[21] Y. Keller and Y. Shkolnisky, "A Signal Processing Approach to Symmetry Detection," *IEEE Trans. Image Processing,* vol. 15, no. 6, pp. 2198-2207, Aug. 2006.
[22] S. Lee, R. Collins, and Y. Liu, "Rotation Symmetry Group Detection via Frequency Analysis of Frieze-Expansions," *Proc. IEEE Computer Vision and Pattern Recognition Conf.,* June 2008.
[23] Y. Lei and K. Wong, "Detection and Localisation of Reflectional and Rotational Symmetry under Weak Perspective Projection," *Pattern Recognition,* vol. 32, no. 2, pp. 167-180, Feb. 1999.
[24] H. Zabrodsky, S. Peleg, and D. Avnir, "Symmetry as a Continuous Feature," *IEEE Trans. Pattern Analysis and Machine Intelligence,* vol. 17, no. 12, pp. 1154-1166, Dec. 1995.
[25] V.S.N. Prasad and B. Yegnanarayana, "Finding Axes of Symmetry from Potential Fields," *IEEE Trans. Image Processing,* vol. 13, no. 12, pp. 1559-1566, Dec. 2004.
[26] A. Martinet, C. Soler, N. Holzschuch, and F. Sillion, "Accurate Detection of Symmetries in 3D Shapes," *ACM Trans. Graphics,* vol. 25, no. 2, pp. 439-464, Apr. 2006.
[27] T. Ojala, M. Pietikäinen, and T. Mäenpää, "Multiresolution Gray-Scale and Rotation Invariant Texture Classification with Local Binary Patterns," *IEEE Trans. Pattern Analysis and Machine Intelligence,* vol. 24, no. 7, pp. 971-987, July 2002.
[28] J.H. Hays, M. Leordeanu, A.A. Efros, and Y. Liu, "Discovering Texture Regularity via Higher-Order Matching," *Proc. Ninth European Conf. Computer Vision,* pp. 522-535, May 2006.
[29] J. Zhang, M. Marszalek, S. Lazebnik, and C. Schmid, "Local Features and Kernels for Classification of Texture and Object Categories: A Comprehensive Study," *Int'l J. Computer Vision,* vol. 73, no. 2, pp. 213-238, 2007.
[30] M. Brown and D.G. Lowe, "Recognising Panoramas," *Proc. IEEE Int'l Conf. Computer Vision,* vol. 2, pp. 1218-1227, 2003.
[31] F. Tang and H. Tao, "Object Tracking with Dynamic Feature Graph," *Proc. Performance Evaluation and Tracking of Surveillance,* pp. 25-32, 2005.
[32] K. Mikolajczyk and C. Schmid, "Scale and Affine Invariant Interest Point Detectors," *Int'l J. Computer Vision,* vol. 60, no. 1, pp. 63-86, Oct. 2004.
[33] K. Mikolajczyk, T. Tuytelaars, C. Schmid, A. Zisserman, J. Matas, F. Schaffalitzky, T. Kadir, and L. Van Gool, "A Comparison of Affine Region Detectors," *Int'l J. Computer Vision,* vol. 65, nos. 1/2, pp. 43-72, 2005.
[34] J. Matas, O. Chum, M. Urban, and T. Pajdla, "Robust Wide Baseline Stereo from Maximally Stable Extremal Regions," *Proc. British Machine Vision Conf.,* pp. 384-393, 2002.
[35] M.-E. Nilsback and A. Zisserman, "A Visual Vocabulary for Flower Classification," *Proc. IEEE Conf. Computer Vision and Pattern Recognition,* 2006.
[36] G. Scott and H. Longuet Higgins, "An Algorithm for Associating the Features of Two Images," *Proc. Royal Soc. London,* vol. B-244, pp. 21-26, 1991.
[37] A.C. Berg, T.L. Berg, and J. Malik, "Shape Matching and Object Recognition Using Low Distortion Correspondences," *Proc. IEEE Conf. Computer Vision and Pattern Recognition,* vol. 1, pp. 26-33, June 2005.
[38] J. Shi and J. Malik, "Normalized Cuts and Image Segmentation," *IEEE Trans. Pattern Analysis and Machine Intelligence,* vol. 22, no. 8, pp. 888-905, Aug. 2000.
[39] T. Cour, P. Srinivasan, and J. Shi, "Balanced Graph Matching," *Advances in Neural Information Processing Systems,* B. Schölkopf, J. Platt, and T. Hoffman, eds., vol. 19, pp. 313-320, MIT Press, 2007.
[40] Y. Eldar, M. Lindenbaum, M. Porat, and Y. Zeevi, "The Farthest Point Strategy for Progressive Image Sampling," *IEEE Trans. Image Processing,* vol. 6, no. 9, pp. 1305-1315, Sept. 1997.
[41] R.I. Hartley and A. Zisserman, *Multiple View Geometry in Computer Vision,* second ed. Cambridge Univ. Press, 2004.
[42] M. Fischler and R. Bolles, "Random Sample Consensus: A Paradigm for Model Fitting with Applications to Image Analysis and Automated Cartography," *Comm. ACM,* vol. 24, no. 6, pp. 381-395, June 1981.
[43] "Bioid, the Bioid Face Database," http://www.bioid.com/downloads/facedb/, 2001.
[44] M. Valstar and M. Pantic, "Fully Automatic Facial Action Unit Detection and Temporal Analysis," *Proc. IEEE Int'l Conf. Computer Vision and Pattern Recognition,* vol. 3, May 2006.

Michael Chertok received the BSc degree in computer engineering in 1998 from the Technion-Israel Institute of Technology, Haifa. He is currently pursuing the PhD degree in electrical engineering at Bar-Ilan University, Israel. He has vast industry experience in computer vision and image processing. His research interests include data analysis using graphs and computer vision.

Yosi Keller received the BSc degree in electrical engineering in 1994 from the Technion-Israel Institute of Technology, Haifa, and the MSc and PhD degrees in electrical engineering from Tel-Aviv University in 1998 and 2003, respectively. From 1994 to 1998, he was an R&D officer in the Israeli Intelligence Force. From 2003 to 2006, he was a Gibbs assistant professor with the Department of Mathematics at Yale University. He is a senior lecturer in the Electrical Engineering Department at Bar-Ilan University, Israel. His research interests include graph-based data analysis and optimization and spectral-graph-theory-based dimensionality reduction.